Available online at www.sciencedirect.com
SCIENCE DIRECT®
Journal of Solid State Chemistry 177 (2004) 806–816
JOURNAL OF SOLID STATE CHEMISTRY
http://elsevier.com/locate/jssc

# Layered perovskite-related ruthenium oxychlorides: crystal structure of two new compounds $Ba_5Ru_2Cl_2O_9$ and $Ba_6Ru_3Cl_2O_{12}$

N. Tancret, P. Roussel, and F. Abraham*

*Laboratoire de Cristallochimie et Physiochimie du Solide, UMR CNRS 8012 ENSC, Université de Sciences et Technique de Lille, BP 108, Villeneuve d'Ascq Cedex 59652, France*

Received 18 June 2003; received in revised form 11 September 2003; accepted 17 September 2003

**Abstract**

Single crystals of the title compounds were prepared using a $BaCl_2$ flux and investigated by X-ray diffraction methods using Mo$K\alpha$ radiation and a charge coupled device (CCD) detector. The crystal structures of these two new compounds were solved and refined in the hexagonal symmetry with space group $P6_3/mmc$, $a = 5.851(1)$ Å, $c = 25.009(5)$ Å, $\rho_{cal} = 4.94\,g\,cm^{-3}$, $Z = 2$ to a final $R_1 = 0.069$ for 20 parameters with 312 reflections for $Ba_5Ru_2Cl_2O_9$ and space group $P\bar{3}m1$, $a = 5.815(1)$ Å, $c = 14.915(3)$ Å, $\rho_{cal} = 5.28\,g\,cm^{-3}$, $Z = 1$ to a final $R_1 = 0.039$ for 24 parameters with 300 reflections for $Ba_6Ru_3Cl_2O_{12}$. The structure of $Ba_5Ru_2Cl_2O_9$ is formed by the periodic stacking along [001] of three hexagonal close-packed $BaO_3$ layers separated by a double layer of composition $Ba_2Cl_2$. The $BaO_3$ stacking creates binuclear face-sharing octahedra units $Ru_2O_9$ containing Ru(V). The structure of $Ba_6Ru_3Cl_2O_{12}$ is built up by the periodic stacking along [001] of four hexagonal close-packed $BaO_3$ layers separated by a double layer of composition $Ba_2Cl_2$. The ruthenium ions with a mean oxidation degree +4.67 occupy the octahedral interstices formed by the four layers hexagonal perovskite slab and then constitute isolated trinuclear $Ru_3O_{12}$ units. These two new oxychlorides belong to the family of compounds formulated as $[Ba_2Cl_2][Ba_{n+1}Ru_nO_{3n+3}]$, where $n$ represents the thickness of the octahedral string in hexagonal perovskite slabs.


*Keywords:* Ruthenium oxychloride; Hexagonal perovskite; Crystal structure

## 1. Introduction

Numerous compounds with structure considered as perovskite related demonstrate unusual and interesting properties such as ferroelectricity, oxide-ion conductivity, high-temperature superconductivity, colossal magnetoresistivity, and catalytic activity. In many of these compounds cubic-type perovskite anionic layers of formula $[A_{n-1}M_nO_{3n+1}]$, where $n$ denotes the thickness of the layers in terms of $MO_6$ octahedra, are interleaved with positively charged layers leading to tetragonal or pseudotetragonal symmetry with an $a$-lattice parameter of the order of $a_p$ ($a_p$ = simple cubic perovskite unit-cell parameter). The main families are obtained for "fluorite-like" $[Bi_2O_2]^{2+}$ layers (the Aurivillius series [1]) and rock-salt layers (the Dion—Jacobson [2] and the Ruddelsden–Popper series [3] for single $[A'O]$ and double $[A'O]_2$ rock-salt layers, respectively) as cationic layers between the perovskite-type slices. The cubic perovskite and the cubic perovskite-type layers can be described by the stacking of compact hexagonal $AO_3$ layers in a sequence of **abc**, the small cations, $B$, occupying octahedral holes between the layers, the $BO_6$ octahedra sharing only corners. Hexagonal close packed in a sequence **ab** can be introduced in the stacking, leading to a huge quantity of various stacking sequences from entirely cubic (corner-shared octahedra) to entirely hexagonal (face-shared octahedra), depending on the size of both $A$ and $B$ ions and synthetic conditions. A typical example is $BaRuO_3$ which adopts different polytype structures depending on the synthetic conditions [4]. At atmospheric pressure, $BaRuO_3$ has a 9R structure with $(hhc)_3$ stacking sequence and contains $Ru_3O_{12}$ trimers of face-shared octahedra linked together by corner sharing. At 15 kbar, $BaRuO_3$ transforms to a 4H structure with $(hc)_2$ stacking sequence and contains $Ru_2O_9$ dimers of face-shared octahedra linked together

*Corresponding author. Fax: +33-03-20-43-48-14.
*E-mail address:* francis.abraham@ensc-lille.fr (F. Abraham).

0022-4596/$ - see front matter © 2003 Elsevier Inc. All rights reserved.
doi:10.1016/j.jssc.2003.09.014

by corner sharing. At 30 kbar, this structure transforms to a 6H structure with $(hcc)_2$ stacking sequence and contains $Ru_2O_9$ dimers of face-shared octahedra linked by corner sharing with a layer of isolated octahedra. Finally, a cubic 3C perovskite structure is expected for $BaRuO_3$ at about 120 kbar [4]. Various types of $[A_nX_m]$ layers with $(n+m\leqslant 4)$ can be introduced in the $[AO_3]$ stacking sequence leading to many original structures having hexagonal or rhombohedral symmetry with an $a$-lattice parameter of the order of $a_p\sqrt{2}$ and a $c$-parameter related to the stacking sequence (for a review, see Ref. [5]). Depending on the nature and the stoichiometry of the $[A_nX_m]$ layer, different intergrowth structures are obtained in which hexagonal perovskite $[A_{n+1}M_nO_{3n+3}]$ slices of $n$ octahedra thickness are connected through various polyhedra sheets such as trigonal pyramids in the $Ba_3M_4O_9$ ($M$ = Sc, Y, $Ln$ = Dy–Lu) compounds [6] or pairs of corner-shared tetrahedra in, for example, $\beta$-$Ba_2ScAlO_5$ [7], $Ba_5In_2Al_2ZrO_{13}$ [8] and $Ba_5Co_5ClO_{13}$ [9] and isotypic oxychlorides [10]. In other interesting cases, the $[A_{n+1}M_nO_{3n+3}]$ slabs are separated by cationic layers such as $[Ba_2O]$ in $Ba_5Ru_2O_{10}$ [11,12], $[Ba_2(O_2)]$ in $Ba_5Ru_2O_9O_2$ [12,13] containing peroxide anions, or $[Ba_2Cl]$ in $Ba_5Ru_2O_9Cl$ [14] or by double "rock salt-type" cationic layers $[BaCl]_2$. In this last example, oxychlorides formulated $[Ba_2Cl_2]$ $[Ba_{n+1}M_nO_{3n+3}]$ have already been reported for $n=2$ ($Ba_5RuTaO_9Cl_2$ [15] and $Ba_5Ru_{1.6}W_{0.4}O_9Cl_2$ [16]), for $n=3$ ($Ba_6Ru_2PtO_{12}Cl_2$ [17], $Ba_6Ru_{2.5}Mn_{0.5}O_{12}Cl_2$ [18] and $Ba_6Nb_2IrO_{12}Cl_2$ [19]), for $n=4$ ($Ba_7Ru_4O_{15}Cl_2$ [20]) and for $n=5$ ($Ba_8Ru_{3.33}Ta_{1.67}O_{18}Cl_2$ [21]). Astonishingly, only the term $n=4$ has been reported for ruthenium as the unique $M$ cation in the octahedral interstices of the $[BaO_3]$ layers stacking. In the present paper, we described the crystal structure of the ruthenium oxychlorides $Ba_5Ru_2Cl_2O_9$ and $Ba_6Ru_3Cl_2O_{12}$ which adopt hexagonal 10- and 12-layers structures, respectively. A comparison is made with other barium ruthenium oxides and oxyhalides and in particular with an other form of $Ba_5Ru_2Cl_2O_9$ which has a very different structure [22].

## 2. Experimental

The starting materials, $BaCl_2\cdot 2H_2O$ (Prolabo, Rectapur, 99%), $BaCO_3$ (Fisher, 99%) and Ru (Touzart & Matignon, 99%), were used as received. Several compositions of these reactants were mixed and heated at different temperatures between 1000°C and 1100°C (Table 1). After cooling to room temperature and dissolving the excess of $BaCl_2$ with hot water, black hexagonal-plate crystal pieces were found in most of the experiments. For each synthesis, several single crystals were tested on a single-crystal X-ray diffractometer. Hexagonal unit cells were always obtained with the same $a$-parameter ($a\approx 5.8$ Å) and a $c$-parameter depending on the synthesis conditions allowing the identification of the synthesized single crystals (Table 1). Several crystals were analyzed by energy dispersive spectroscopy using a JEOL JSM-5300 scanning microscope equipped with a PGT Digital Spectrometer, confirming the presence of Ba, Ru and Cl, except for the $BaRuO_3$ crystals, where no chlorine was found.

Table 1
Single-crystal synthesis conditions

| $BaCO_3$/Ru/$BaCl_2\cdot 2H_2O$ ratio | Temperature (°C)/time(h)/cooling rate (°C/h) | Obtained single crystals |
|---|---|---|
| 3/3/10 | 1100/48/24 | $Ba_5Ru_2Cl_2O_9$ |
| 3/1/10 | 1050/24/quenching | $Ba_6Ru_3Cl_2O_{12}$ |
| 5/2/10 | 1000/80/quenching | $BaRuO_3+Ba_7Ru_4Cl_2O_{15}$ |
| 5/2/10 | 1100/48/24 | $Ba_7Ru_4Cl_2O_{15}$ |
| 3/1/6 | 1100/48/24 | $Ba_7Ru_4Cl_2O_{15}$ |

### 2.1. Crystal structure determination

For structure determinations, crystals of $Ba_5Ru_2Cl_2O_9$ and $Ba_6Ru_3Cl_2O_{12}$ were selected, mounted on glass fibers and aligned on a Bruker SMART CCD X-ray diffractometer. Intensities were collected at room temperature using Mo$K\alpha$ ($\lambda=0.71073$ Å) radiation selected by a graphite monochromator. The individual frames were measured using a $\omega$-scan technique with an omega rotation of 0.3° and an acquisition time of 20 s per frame. A total of 1800 frames were collected covering the full sphere. After every data collection, the intensity data were integrated and corrected for Lorentz, polarization and background effects using the Bruker program SAINT [23]. Once the data processing was performed, the absorption corrections were computed using a semi-empirical method based on redundancy with the SADABS program [24]. Details of the data collection and refinement are given in Table 2. The hexagonal unit-cell parameters were refined to $a=5.851(1)$ Å, $c=25.009(5)$ Å and $a=5.815(1)$ Å, $c=14.915(3)$ Å for $Ba_5Ru_2Cl_2O_9$ and $Ba_6Ru_3Cl_2O_{12}$, respectively.

Crystal structures were determined in the centrosymmetric $P6_3/mmc$ and $P\bar{3}m1$ space groups for $Ba_5Ru_2Cl_2O_9$ and $Ba_6Ru_3Cl_2O_{12}$, respectively, by direct methods using SIR97 program [25], which readily established the heavy atom positions (Ba, Ru, Cl). Oxygen atoms were localized from difference Fourier maps. The last cycles of refinement included atomic positions, anisotropic displacement parameters for all non-oxygen atoms, and isotropic displacement parameters for oxygen atoms. Full-matrix least-squares structure refinements against F were carried out using the JANA2000 [26] program.

Table 2
Crystal data, intensity collection and structure refinement parameters for $Ba_5Ru_2Cl_2O_9$ and $Ba_6Ru_3Cl_2O_{12}$

| | $Ba_5Ru_2Cl_2O_9$ | $Ba_6Ru_3Cl_2O_{12}$ |
|---|---|---|
| *Crystallographic data* | | |
| Formula weight ($g\,mol^{-1}$) | 1103.74 | 1390.15 |
| Crystal system | Hexagonal | Hexagonal |
| Space group | $P6_3/mmc$ | $P\bar{3}m1$ |
| Unit-cell dimensions (Å) | $a = 5.851(1)$ | $a = 5.815(1)$ |
| | $c = 25.009(5)$ | $c = 14.915(3)$ |
| Cell volume (Å$^3$) | 741.5(4) | 436.8(2) |
| $Z$ | 2 | 1 |
| Density, calculated ($g\,cm^{-3}$) | 4.94 | 5.28 |
| $F(000)$ | 948 | 598 |
| *Intensity collection* | | |
| Wavelength (Å) | 0.71073 (Mo$K\alpha$) | 0.71073 (Mo$K\alpha$) |
| $\theta$ range (deg) | 3.26–28.77 | 4.05–23.27 |
| Data collected | $-7 \leqslant h \leqslant 7$ | $-6 \leqslant h \leqslant 6$ |
| | $-7 \leqslant k \leqslant 7$ | $-6 \leqslant k \leqslant 6$ |
| | $-32 \leqslant l \leqslant 32$ | $-16 \leqslant l \leqslant 16$ |
| No. of reflections measured | 4553 | 2320 |
| No. of independent reflections | 421 | 416 |
| Redundancy | 10.81 | 5.58 |
| No. of unique reflections ($I > 3\sigma(I)$) | 312 | 300 |
| $\mu$ (Mo$K\alpha$) ($mm^{-1}$) | 15.416 | 16.786 |
| $T_{max}/T_{min}$ | 0.491 | 0.526 |
| $R(F^2)_{int}$ | 0.0599 | 0.0472 |
| *Refinement* | | |
| No. of parameters | 20 | 24 |
| Weighting scheme | $1/\sigma^2$ | $1/\sigma^2$ |
| $R(F)$ obs/all | 0.0609/0.0886 | 0.0391/0.0572 |
| w$R(F)$ obs/all | 0.0586/0.0591 | 0.0454/0.0457/ |
| Max, min $\Delta\rho$(e Å$^{-3}$) | 7.75/−7.89 | 5.48/−2.20 |

Table 3
Atomic coordinates and isotropic displacement parameters of $Ba_5Ru_2Cl_2O_9$

| Atom | Wyck. | $x$ | $y$ | $z$ | $U_{eq}$ or $U_{iso}$ | |
|---|---|---|---|---|---|---|
| Ba(1) | 2*d* | 1/3 | 2/3 | 3/4 | 0.0114(8) | |
| Ba(2) | 4*f* | 1/3 | 2/3 | 0.33041(8) | 0.0144(6) | |
| Ba(3) | 4*f* | 1/3 | 2/3 | 0.57753(9) | 0.0282(7) | |
| Ru | 4*e* | 0 | 0 | 0.30636(11) | 0.0097(6) | |
| Cl | 4*f* | 1/3 | 2/3 | 0.4517(5) | 0.091(6) | |
| O(1) | 6*h* | 0.150(1) | 0.299(3) | 1/4 | 0.009(4) | |
| O(2) | 12*k* | 0.321(2) | 0.160(1) | 0.3441(5) | 0.017(3) | |
| | $U_{11}$ | $U_{22}$ | $U_{33}$ | $U_{12}$ | $U_{13}$ | $U_{23}$ |
| Ba(1) | 0.0063(9) | 0.0063(9) | 0.021(2) | 0.0031(4) | 0 | 0 |
| Ba(2) | 0.0118(7) | 0.0118(7) | 0.019(1) | 0.0059(3) | 0 | 0 |
| Ba(3) | 0.0314(9) | 0.0314(9) | 0.022(1) | 0.0157(5) | 0 | 0 |
| Ru | 0.0066(7) | 0.0066(7) | 0.016(1) | 0.0033(3) | 0 | 0 |
| Cl | 0.124(9) | 0.124(9) | 0.026(7) | 0.062(4) | 0 | 0 |

*Note*. The $U_{eq}$ values are defined by $U_{eq} = 1/3(\sum_i \sum_j U_{ij} a_i^* a_j^* a_i a_j)$. The anisotropic displacement factor exponent takes the form $-2\pi^2[h^2 a^{*2} U_{11} + \cdots + 2hka^* b^* U_{12}]$.

## 3. Crystal structure description and discussion

### 3.1. $Ba_5Ru_2Cl_2O_9$

The atomic coordinates and displacement parameters for $Ba_5Ru_2Cl_2O_9$ are given in Table 3. Selected bond lengths are listed in Table 4. Valence bond sums also reported in Table 4 were calculated using the expression of bond valence $S_{ij}$ between two atoms $i$ and $j$ given by Brown [27], $S_{ij} = \exp(R_0 - R_{ij})/b$ were $R_{ij}$ are the observed bond distances and $R_0$ and $b$ are empirical constants. For these calculations, $R_0$ parameters listed by Brese and O'Keeffe's data [28] were used except for $Ru^V$–O bonds where the $R_0$ parameter ($R_0 = 1.888$ Å) was taken from Dussarat et al. [29]. $b$ was fixed to the commonly taken value, $b = 0.37$ Å [30]. The structure of $Ba_5Ru_2Cl_2O_9$ is shown in Fig. 1. It can be described as a perovskite-related compound with a 10-layer stacking along the $c$-axis of $BaO_3$ and BaCl layers in the sequence $(h'hhhh')_2$, where $h$ is an hexagonal $BaO_3$ layer and $h'$ a BaCl layer, still termed as hexagonal because of the Ba positions. The Cl atoms occupy the center of half the $O_3$ triangles of a $BaO_3$ layer (Fig. 1), while the ruthenium atom occupy the octahedral sites created by the three $BaO_3$ layers, leading to the formation of $Ru_2O_9$ dimers of face-shared octahedra. Thus the structure can be described as resulting of the intergrowth of hexagonal perovskite-type blocks $(Ba_3Ru_2O_9)^{2-}$ with rock salt-type double layers $(Ba_2Cl_2)^{2+}$. This compound is isostructural with $Ba_5Ru_{1.6}W_{0.4}Cl_2O_9$ [16] and $Ba_5RuTaCl_2O_9$ [15] even if the last compound has been refined in the non-centrosymmetric $P6_322$ space group, the difference involving only the O(2) oxygen atom coordinates. In $Ba_5Ru_{1.6}W_{0.4}Cl_2O_9$ and $Ba_5RuTaCl_2O_9$ the Ru and $M$ atoms ($M$ = W, Ta) are disordered on the two octahedral sites of the $(Ru,M)_2O_9$ dimeric units.

In $Ba_5Ru_2Cl_2O_9$ the calculated valence bond sum for Ru (4.90) is in good agreement with the expected value of 5 deduced from electroneutrality. The distance between the two Ru(V) within the $Ru_2O_9$ dimer (2.819(4) Å) is shorter than the distance observed in the disordered $(Ru,M)_2O_9$ units in the isostructural compounds, 2.872 and 2.944 Å for $M$ = W and Ta, respectively. This value is intermediate between the Ru−Ru distances reported in $Ru_2O_{10}$ pairs of edge-shared octahedra with strong metal–metal bonding in $La_4Ru_6O_{19}$ [31] (2.488 Å) and no metal–metal bonding in $La_3Ru_3O_{11}$ [32] (2.990 Å). In numerous ruthenium oxides containing $Ru_2O_9$ pairs of face-shared octahedra, hereafter FSO, the Ru–Ru bond length is strongly related to the mean oxidation degree (MOD) of Ru (Table 5). The main series with formula $Ba_3MRu_2O_9$ with $M$ a mono-, di-, tri- or tetravalent metal adopts the 6H-$(cch)_2$ perovskite-related structure, the $Ru_2O_9$ pairs are connected by corner sharing with a single layer of $MO_6$ isolated octahedra (Fig. 2a). For $M^{4+}$ cations, compounds are known for $M$ = Ce, Pr, Tb [33] and

Table 4
Bond distances (Å) and bond valences $S_{ij}$ in $Ba_5Ru_2Cl_2O_9$

| | | $S_{ij}$ | | | $S_{ij}$ |
|---|---|---|---|---|---|
| Ba(1)–O(1) (6 ×) | 2.93(1) | | Ru–Ru | 2.819(4) | |
| Ba(1)–O(2) (6 ×) | 2.94(1) | 0.173 | Ru–O(1) (3 ×) | 2.07(1) | 0.611 |
| | $\sum S_{ij}$ = | 2.100 | Ru–O(2) (3 ×) | 1.88(1) | 1.022 |
| Ba(2)–O(1) (3 ×) | 2.74(1) | 0.296 | | $\sum S_{ij}$ = | 4.899 |
| Ba(2)–O(2) (6 ×) | 2.95(1) | 0.164 | O(1)–O(1) (2 ×) | 2.62(2) | |
| Ba(2)–Cl (1 ×) | 3.03(1) | 0.399 | O(1)–O(2) (4 ×) | 2.83(1) | |
| | $\sum S_{ij}$ = | 2.271 | O(2)–O(2) (2 ×) | 2.81(2) | |
| Ba(3)–O(2) (3 ×) | 2.63(1) | 0.399 | | | |
| Ba(3)–Cl (3 ×) | 3.46(1) | 0.125 | | | |
| Ba(3)–Cl (1 ×) | 3.15(1) | 0.288 | | | |
| | $\sum S_{ij}$ = | 1.860 | | | |
| O(1)–Ba(1) (2 ×) | 2.93(1) | 0.177 | O(2)–Ba(1) | 2.94(1) | 0.173 |
| O(1)–Ba(2) (2 ×) | 2.74(1) | 0.296 | O(2)–Ba(2) (2 ×) | 2.95(1) | 0.164 |
| O(1)–Ru (2 ×) | 2.07(1) | 0.611 | O(2)–Ba(3) (2 ×) | 2.63(1) | 0.399 |
| | $\sum S_{ij}$ = | 2.168 | O(2)–Ru | 1.88(1) | 1.022 |
| Cl–Ba(2) | 3.03(1) | 0.399 | | $\sum S_{ij}$ = | 1.925 |
| Cl–Ba(3) | 3.15(1) | 0.288 | | | |
| Cl–Ba(3) (3 ×) | 3.46(1) | 0.125 | | | |
| | $\sum S_{ij}$ = | 1.062 | | | |

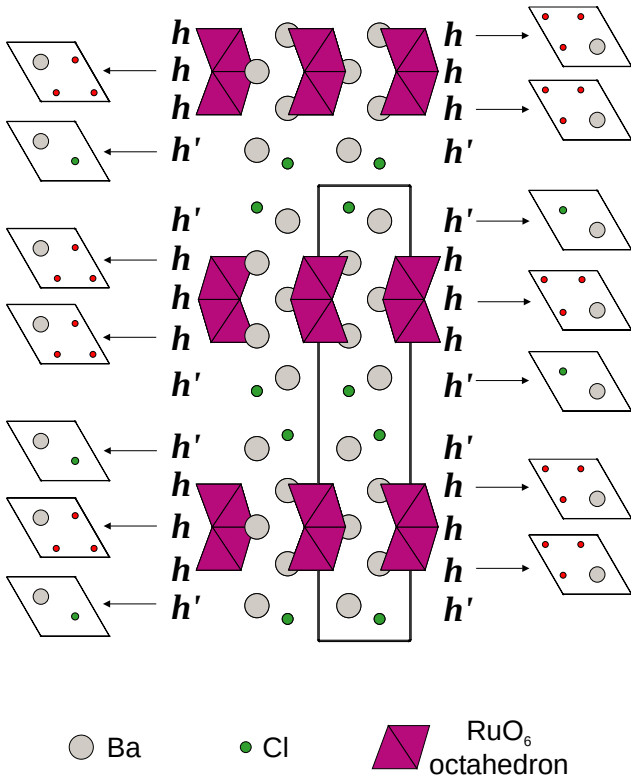


Fig. 1. Projection along [010] of the crystal structure of $Ba_5Ru_2Cl_2O_9$ with the $BaO_3$ and BaCl layers stacked along [001].

$M$ = Ti [34]. In those compounds, the ruthenium is Ru(IV), the usual oxidation state of Ru, and the metal–metal bond is strong, the Ru–Ru distance being in the range 2.48–2.52 Å, is significant smaller than in the metal itself (2.65 Å) and comparable with the value in $La_4Ru_6O_{19}$ [31]. However, the distance remains significantly greater than the distance between two $BaO_3$ layers (about 2.4 Å). For $M^{3+}$, $Ba_3MRu_2O_9$ compounds have been reported for all the other lanthanide ions [35–38] and for $M$ = Y, In [35,37,39], the MOD of Ru is +4.5 and the metal–metal bond remains strong, the Ru–Ru distance is in the range 2.52–2.56 Å. For $M^{2+}$ cations ($M$ = Ni, Co, Zn, Cu [36,39,40] and $M$ = Mg, Ca, Cd, Sr [41–43]), the ruthenium is Ru(V), the metal–metal bond, although weaker, remains strong (the Ru–Ru distance is in the range 2.65–2.70 Å). Finally, a compound of this series with $M^+ = Na^+$ has been recently characterized [44,45], the MOD of Ru is +5.5 and the metal–metal distance is significantly longer (2.745 Å). Thus the Ru–Ru distance within the FSO dimer in this large isostructural series increases with the oxidation degree of the ruthenium atom in accordance with the electrostatic repulsion between the charged cations. The sequence of $BaO_3$ layers in 4H-$BaRuO_3$ is $(ch)_2$, the $Ru_2O_9$ dimers are linked together directly by corner sharing (Fig. 2b), the intradimer Ru–Ru distance (2.537(1) Å) [46] is slightly out of the range previously discussed for Ru(IV). In $Ba_4NaRu_3O_{12}$ [47] which adopts a 8H structure with a $(ccch)_2$ stacking sequence the $Ru_2O_9$ pairs are linked together by corner sharing with a double layer of vertex-shared $NaO_6$ and $RuO_6$ octahedra (Fig. 2c); the Ru–Ru distance within the pair (2.66(2) Å) is in the range reported for Ru(V) in the $Ba_3MRu_2O_9$ series. $Ba_2BiRuO_6$ crystallize with a similar distorted 8H structure [48] and the Ru–Ru distance (2.679(5) Å) within the $Ru_2O_9$ pairs linked by a double layer of corner-shared $BiO_6$ octahedra (Fig. 2d) is also in the range for Ru(V) and close to the value calculated in $Ba_5Na_2Ru_3O_{14}$ (2.676(1) Å) [49]. In this last compound, $Ru(V)_2O_9$ pairs are linked through corner sharing by

Table 5
Compounds containing $Ru_2O_9$ dimers made from face-shared $RuO_6$ octahedra

| Compound | | MOD for Ru | Ru–Ru | Structure | Ref |
|---|---|---|---|---|---|
| $Ba_3M^{4+}Ru_2O_9$ | $M$=Ce | 4 | 2.481(3) | 6H-$(hcc)_2$ | [33] |
| | $M$=Pr | 4 | 2.486(2) | 6H-$(hcc)_2$ | [33] |
| | $M$=Tb | 4 | 2.493(6) | 6H-$(hcc)_2$ | [33] |
| | $M$=Ti | 4 | 2.515(6) | 6H-$(hcc)_2$ | [34] |
| $Ba_3M^{3+}Ru_2O_9$ | $M$=Y | 4.5 | 2.540(2)/2.526(5) | 6H-$(hcc)_2$ | [35,37] |
| | $M$=In | 4.5 | 2.563(4)/2.517(7) | 6H-$(hcc)_2$ | [35,39] |
| | $M$=La | 4.5 | 2.554(3) | 6H-$(hcc)_2$ | [35] |
| | $M$=Sm | 4.5 | 2.536(3) | 6H-$(hcc)_2$ | [35] |
| | $M$=Eu | 4.5 | 2.537(4) | 6H-$(hcc)_2$ | [35] |
| | $M$=Lu | 4.5 | 2.549(3) | 6H-$(hcc)_2$ | [35] |
| | $M$=Gd | 4.5 | 2.527(3)/2.534(5) | 6H-$(hcc)_2$ | [36,37] |
| | $M$=Ho | 4.5 | 2.547(3) | 6H-$(hcc)_2$ | [36] |
| | $M$=Er | 4.5 | 2.545(3) | 6H-$(hcc)_2$ | [36] |
| | $M$=Tb | 4.5 | 2.543(3) | 6H-$(hcc)_2$ | [36] |
| | $M$=Yb | 4.5 | 2.547(3)/2.541(3) | 6H-$(hcc)_2$ | [36,37] |
| | $M$=Nd | 4.5 | 2.524(4) | 6H-$(hcc)_2$ | [38] |
| $Ba_3M^{2+}Ru_2O_9$ | $M$=Ni | 5 | 2.681(2)/2.686(4) | 6H-$(hcc)_2$ | [39,40] |
| | $M$=Co | 5 | 2.677(7)/2.684(4) | 6H-$(hcc)_2$ | [39,40] |
| | $M$=Zn | 5 | 2.685(2) | 6H-$(hcc)_2$ | [40] |
| | $M$=Cu | 5 | 2.701(4) | 6H-$(hcc)_2$ | [39] |
| | $M$=Mg | 5 | | 6H-$(hcc)_2$ | [41] |
| | $M$=Ca | 5 | /2.652 | 6H-$(hcc)_2$ | [41,42] |
| | $M$=Cd | 5 | | 6H-$(hcc)_2$ | [41] |
| | $M$=Sr | 5 | /2.676(6) | 6H-$(hcc)_2$ | [41,43] |
| $Ba_3M^{+}Ru_2O_9$ | $M$=Na | 5.5 | 2.748(2)/2.745(1) | 6H-$(hcc)_2$ | [44,45] |
| 4H-$BaRuO_3$ | | 4 | 2.537(1) | 4H-$(hc)_2$ | [46] |
| $Ba_4NaRu_3O_{12}$ | | 5 | 2.66(2) | 8H-$(hccc)_2$ | [47] |
| $Ba_2BiRuO_6$ | | 5 | 2.679(5) | 8H-$(hccc)_2$ | [48] |
| $Ba_5Na_2Ru_3O_{14}$ | | 5 | 2.676(1) | 10H-$(cchcc)_2$ | [49] |
| $Ba_5Ru_2O_{10}$ | | 5 | 2.735(8) | 8H | [11,12] |
| $Ba_5Ru_2O_9(O)_2$ | | 5 | 2.748(2) | 8H | [12,13] |
| $Ba_5Ru_2O_9Cl$ | | 4.5 | 2.763(3) | 8H | [14] |
| $Ba_6Na_2Ru_2X_2O_{17}$ | $X$=V, Cr, Mn, P, As | 5 | 2.654(4)–2.734(4) | 12H | [50] |

strings of three corner-sharing lacunar $RuO_6$ and $NaO_6$ octahedra; in these strings of three the two outer octahedra are occupied by Na (Fig. 2e), the metal atoms Ru and Na occupying the octahedral sites of a 10H stacking of $BaO_3$ layers with the $(c'chcc')_2$ sequence where $c'$ denotes an oxygen-deficient $BaO_3$ layer [49]. In $Ba_5Ru_2Cl_2O_9$ the $Ru_2O_9$ dimers are no longer linked by corner sharing with octahedra. Indeed, the $[Ba_3Ru_2O_9]^{2-}$ slices containing the $Ru_2O_9$ pairs are separated by $[BaCl]_2$ layers and the Ru(V)–Ru(V) distance is significantly longer (2.819(4) Å) (Fig. 3a). This value is comparable to those calculated in $Ba_5Ru_2O_{10}$ [11,12] and $Ba_5Ru_2O_9(O_2)$ [12,13] in which the double $[Ba_2Cl_2]^{2+}$ layers are substituted by single $[Ba_2O]^{2+}$ and $[Ba_2(O_2)]^{2+}$ layers, respectively (Figs. 3b and c). It is also comparable to the value observed in $Ba_5Ru_2O_9Cl$ [14] where the cationic layer is replaced by a $[Ba_2Cl]^{3+}$ layer (Fig. 3d) leading to a MOD for Ru of +4.5. The recently investigated series $Ba_6Ru_2Na_2X_2O_{17}$ ($X$=V, Cr, Mn, P, As) [50] is also interesting. The $[Ba_3Ru_2O_9]$ slabs containing the FSO $Ru_2O_9$ pairs are flanked on both sides by a layer of $NaO_6$ octahedra that share corners with $XO_4$ tetrahedra (Fig. 3e). In this case, the Ru(V)–Ru(V) distance vary in the range from 2.654 to 2.734 Å depending on the nature of the $X$ atom. Thus, the Ru–Ru distance within the FSO dimer increases with the oxidation degree of the ruthenium atom in accordance with the electrostatic repulsion. However, for Ru(V), for which no metal–metal bond is expected, the Ru–Ru distance is also influenced by the kind of linkage between the dimers and by the chemical nature of the element outside of the dimer-containing layers. Indeed, those elements play a role on the electrostatic attraction of the dimeric ruthenium atoms.

An other variety of $Ba_5Ru_2Cl_2O_9$, orthorhombic, with a drastic different structure has already been published [22]. This structure contains also isolated FSO $Ru_2O_9$

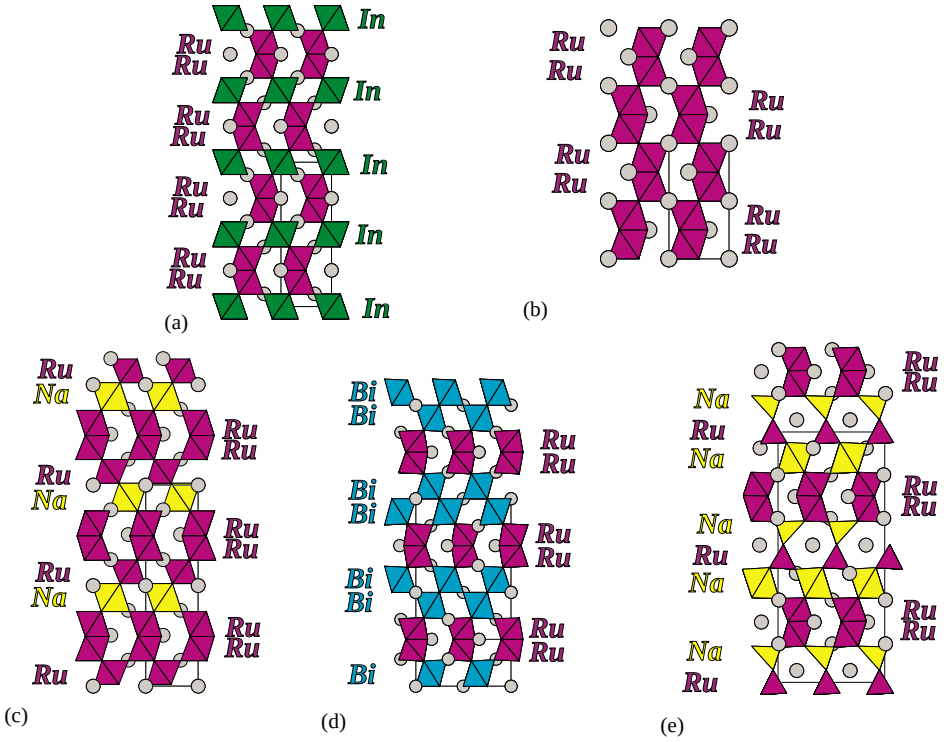


Fig. 2. Crystal structure of hexagonal perovskite-related compounds containing $Ru_2O_9$ dimeric FSO units (a) $Ba_3MRu_2O_9$, (b) 4H-$BaRuO_3$, (c) $Ba_4NaRu_3O_{12}$, (d) $Ba_2BiRuO_6$, and (e) $Ba_5Na_2Ru_3O_{14}$.

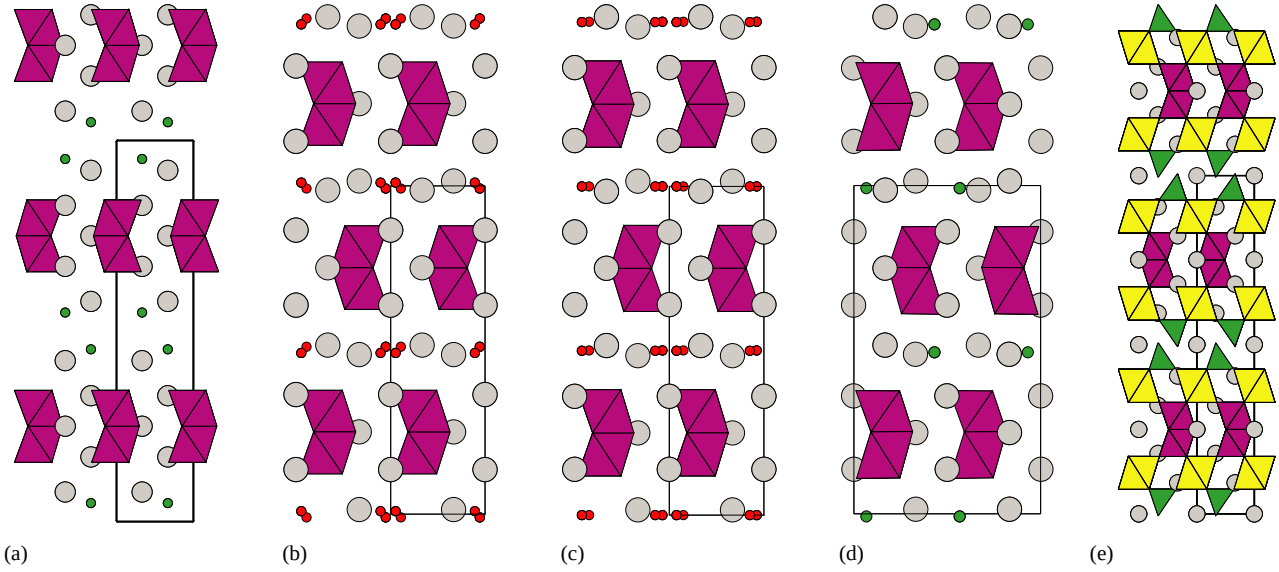


Fig. 3. Crystal structure of hexagonal perovskite-related compounds containing $[Ba_3Ru_2O_9]$ slabs stacked with (a) $[BaCl]_2$ double layers in $Ba_5Ru_2Cl_2O_9$, (b) $[Ba_2O]$ layers in $Ba_5Ru_2O_{10}$, (c) $[Ba_2(O_2)]$ layers in $Ba_5Ru_2O_9(O_2)$, (d) $[Ba_2Cl]$ layers in $Ba_5Ru_2ClO_9$, and (e) complex $Ba_3Na_2X_2O_8$ slabs in $Ba_6Ru_2Na_2X_2O_{17}$.

dimeric units with comparable Ru–Ru distance (2.726 Å) but no layers are apparent (Fig. 4).

In the title compound, the hexagonal $Ba_5Ru_2Cl_2O_9$, the Ba ions are distributed into three crystallographic sites: Ba(1) that pertains to the $BaO_3$ layer at the middle of the $(Ba_3Ru_2O_9)^{2-}$ slab adopts the coordination of metal itself in the hexagonal compact close-packed structure. It can thus be described as an hexagonal capped trigonal prism with twelve oxygen atoms at about 2.93 Å. Ba(2) and Ba(3) are both coordinated by oxide and chloride ions. In the Ba(2) coordination polyhedron, an oxygen triangle is replaced by one

chlorine atom leading to a shortening of the opposite Ba–O bonds (2.74 Å). Moreover, in Ba(3) the six oxygens of the Ba-containing plane are replaced by three chlorine atoms leading to a supplementary shortening of the remaining Ba–O bonds (Fig. 5). The valence bond sums calculated for Ba, O and Cl atoms are consistent with the formal valences of $Ba^{2+}$, $O^{2-}$ and $Cl^{-}$ (Table 4). As already observed in all the compounds containing BaCl layers [15–21], the $U_{11}$ and $U_{22}$ atomic displacement parameters of the chlorine atom are very large corresponding to a high vibration of the Cl in the (001) plane due to the replacement of three oxygen atoms of a $BaO_3$ layer by only one Cl atom at the center of the $O_3$ triangle in a BaCl layer.

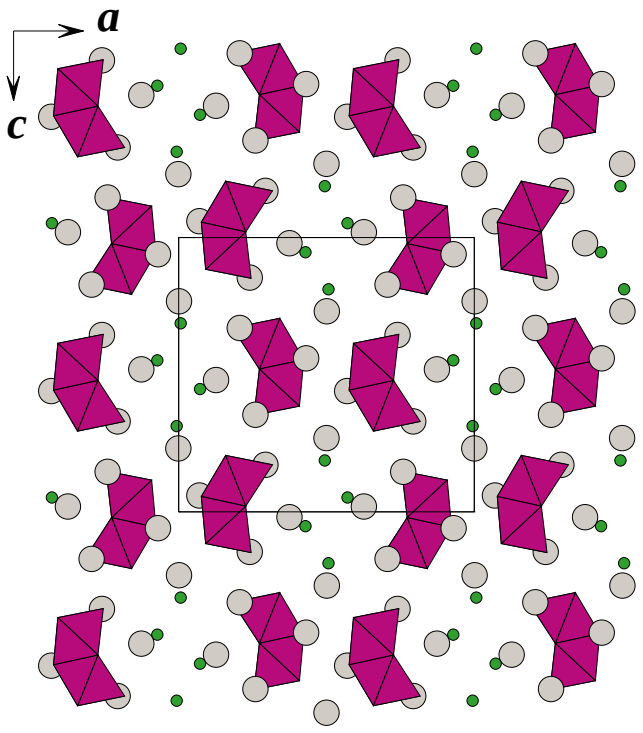


Fig. 4. Crystal structure of orthorhombic $Ba_5Ru_2Cl_2O_9$ view along [010].

### 3.2. $Ba_6Ru_3Cl_2O_{12}$

The atomic coordinates and displacement parameters for $Ba_6Ru_3Cl_2O_{12}$ are given in Table 6. Selected bond lengths with valence bonds are listed in Table 7. The structure of $Ba_6Ru_3Cl_2O_{12}$ is shown in Fig. 6. It is based on a 12-layer $(h'hhhhh')_2$ close-packing along the $c$-axis of $BaO_3$ and BaCl layers. The ruthenium atoms occupy the octahedral sites created by the four $BaO_3$ layers resulting in the formation of $Ru_3O_{12}$ columns of three face-shared octahedra. Thus, the structure can be described as resulting of the intergrowth of hexagonal

Table 6
Atomic coordinates and isotropic displacement parameters of $Ba_6Ru_3Cl_2O_{12}$

| Atom | Wyck. | $x$ | $y$ | $z$ | $U_{eq}$ or $U_{iso}$ |
|---|---|---|---|---|---|
| Ba(1) | 2*d* | 2/3 | 1/3 | 0.9202(1) | 0.0120(7) |
| Ba(2) | 2*d* | 2/3 | 1/3 | 0.2177(2) | 0.0156(7) |
| Ba(3) | 2*d* | 2/3 | 1/3 | 0.6242(1) | 0.0215(8) |
| Ru(1) | 2*c* | 0 | 0 | 0.1780(2) | 0.012(1) |
| Ru(2) | 1*a* | 0 | 0 | 0 | 0.008(2) |
| Cl | 2*d* | 2/3 | 1/3 | 0.4169(9) | 0.068(5) |
| O(1) | 6*i* | 0.162(1) | −0.162(1) | 0.2392(8) | 0.014(3) |
| O(2) | 6*i* | 0.156(1) | −0.156(1) | 0.9184(8) | 0.012(3) |

| | $U_{11}$ | $U_{22}$ | $U_{33}$ | $U_{12}$ | $U_{13}$ | $U_{23}$ |
|---|---|---|---|---|---|---|
| Ba(1) | 0.0076(8) | 0.0076(8) | 0.021(1) | 0.0038(4) | 0 | 0 |
| Ba(2) | 0.0104(8) | 0.0104(8) | 0.026(1) | 0.0052(4) | 0 | 0 |
| Ba(3) | 0.0219(9) | 0.0219(9) | 0.021(2) | 0.0110(5) | 0 | 0 |
| Ru(1) | 0.008(1) | 0.008(1) | 0.020(2) | 0.0040(5) | 0 | 0 |
| Ru(2) | 0.004(1) | 0.004(1) | 0.017(2) | 0.0022(7) | 0 | 0 |
| Cl | 0.086(6) | 0.086(6) | 0.032(8) | 0.043(3) | 0 | 0 |

*Note*. The $U_{eq}$ values are defined by $U_{eq} = 1/3(\sum_i \sum_j U_{ij} a_i^* a_j^* a_i a_j)$. The anisotropic displacement factor exponent takes the form $-2\pi^2[h^2 a^{*2} U_{11} + \cdots + 2hka^* b^* U_{12}]$.

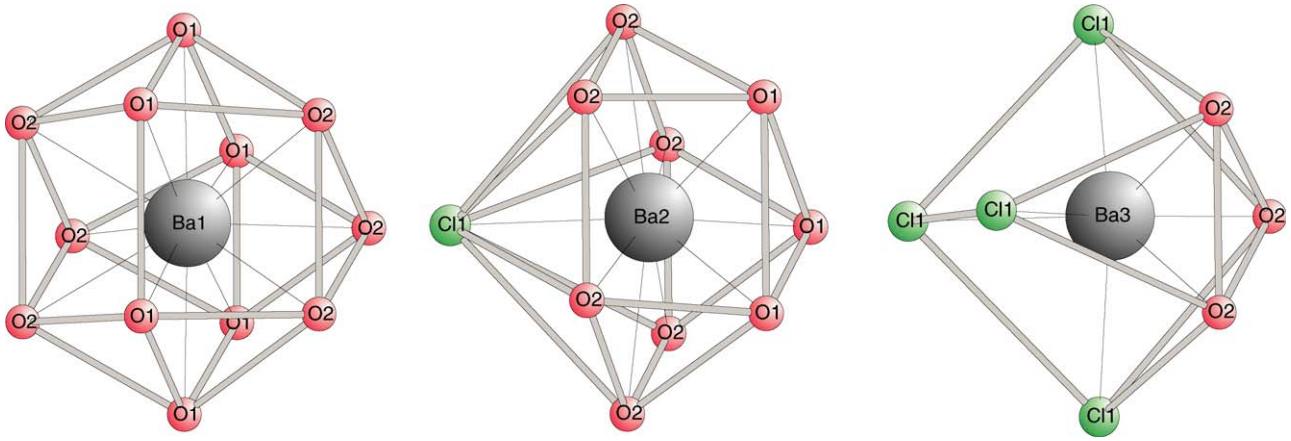


Fig. 5. Schematic view for barium oxychloride and oxide polyhedra of $Ba_5Ru_2Cl_2O_9$: (a) $BaO_{12}$ for Ba(1), (b) $BaO_9Cl$ for Ba(2), and (c) $BaO_3Cl_4$ for Ba(3). The same polyhedra coordination are obtained in $Ba_6Ru_3Cl_2O_{12}$ for Ba(1), Ba(2) and Ba(3), respectively.

Table 7
Bond distances (Å) and bond valences $S_{ij}$ in $Ba_6Ru_3Cl_2O_{12}$

| | | $S_{ij}$ | | | $S_{ij}$ | |
|---|---|---|---|---|---|---|
| | | | | | $Ru^{IV}$ | $Ru^{V}$ |
| Ba(1)–O(1) (3 ×) | 2.94(1) | 0.173 | Ru(1)–Ru(2) | 2.656(3) | | |
| Ba(1)–O(2) (6 ×) | 2.910(5) | 0.187 | | | | |
| Ba(1)–O(2) (3 ×) | 3.00(1) | 0.147 | Ru(1)–O(1) (3 ×) | 1.869(9) | 0.910 | 1.053 |
| | $\sum S_{ij}$ = | 2.082 | Ru(1)–O(2) (3 ×) | 2.13(1) | 0.449 | 0.520 |
| Ba(2)–O(1) (6 ×) | 2.925(8) | 0.180 | | $\sum S_{ij}$ = | 4.077 | 4.72 |
| Ba(2)–O(2) (3 ×) | 2.70(1) | 0.330 | Ru(2)–O(2) (6 ×) | 1.99(1) | 0.656 | 0.759 |
| Ba(2)–Cl (1 ×) | 2.97(1) | 0.469 | | $\sum S_{ij}$ = | 3.936 | 4.554 |
| | $\sum S_{ij}$ = | 2.219 | | | | |
| Ba(3)–O(1) (3 ×) | 2.67(1) | 0.358 | O(1)–O(1) (2 ×) | 2.99(1) | | |
| Ba(3)–Cl (3 ×) | 3.41(1) | 0.143 | O(1)–O(1) (2 ×) | 2.83(1) | | |
| Ba(3)–Cl (1 ×) | 3.09(1) | 0.339 | O(1)–O(2) (2 ×) | 2.85(1) | | |
| | $\sum S_{ij}$ = | 1.840 | O(2)–O(2) (2 ×) | 2.72(1) | | |
| | | | O(2)–O(2) (2 ×) | 2.90(1) | | |

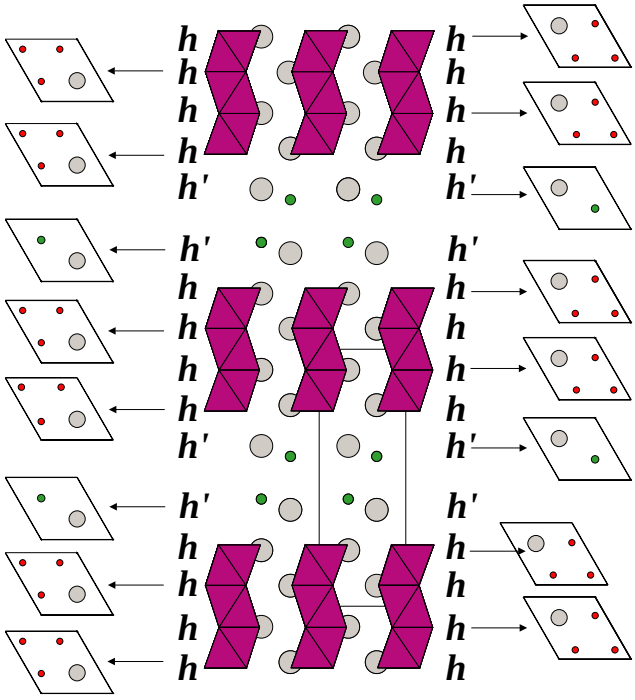


Fig. 6. Projection along [010] of the crystal structure of $Ba_6Ru_3Cl_2O_{12}$ with the $BaO_3$ and BaCl layers stacked along [001].

perovskite blocks $(Ba_4Ru_3O_{12})^{2-}$ with double layer $(Ba_2Cl_2)^{2+}$. This compound is isostructural with $Ba_6Ru_2PtO_{12}Cl_2$ [17], $Ba_6Ru_{2.5}Mn_{0.5}O_{12}Cl_2$ [18] and $Ba_6Nb_2IrO_{12}Cl_2$ [19] where two different metals are disordered on the three octahedral sites of the $M_3O_{12}$ trimeric units. Trimeric FSO $Ru_3O_{12}$ units have been evidenced for the first time in 9R-$BaRuO_3$. The 9R-$BaRuO_3$ structure has been firstly refined by Donohue et al. from single-crystal data collected on precession photographs to $R = 11.8\%$ from 216 independent reflections [51]. Refinements from neutron powder data [52] and X-ray powder data [53] have been recently reported. In the course of our study, good

Table 8
Atomic coordinates and anisotropic displacement parameters of 9R-$BaRuO_3$

| Atom | Wyck. | $x$ | $y$ | $z$ | $U_{eq}$ or $U_{iso}$ |
|---|---|---|---|---|---|
| Ba(1) | 6*c* | −1/3 | 1/3 | 0.05122(5) | 0.0106(3) |
| Ba(2) | 3*b* | 1/3 | −1/3 | 1/6 | 0.0104(3) |
| Ru(1) | 6*c* | 0 | 0 | 0.117029(6) | 0.0077(3) |
| Ru(2) | 3*a* | 0 | 0 | 0 | 0.0081(4) |
| O(1) | 9*d* | 1/3 | 1/6 | 1/6 | 0.013(2) |
| O(2) | 18*h* | −0.3111(9) | −0.1556(5) | 0.0584(2) | 0.009(1) |

| | $U_{11}$ | $U_{22}$ | $U_{33}$ | $U_{12}$ | $U_{13}$ | $U_{23}$ |
|---|---|---|---|---|---|---|
| Ba(1) | 0.0090(3) | 0.0090(3) | 0.0137(5) | 0.0045(2) | 0 | 0 |
| Ba(2) | 0.0082(4) | 0.0082(4) | 0.0146(6) | 0.0041(2) | 0 | 0 |
| Ru(1) | 0.0067(4) | 0.0067(4) | 0.0097(6) | 0.0033(2) | 0 | 0 |
| Ru(2) | 0.0080(5) | 0.0080(5) | 0.0085(8) | 0.0040(3) | 0 | 0 |

Table 9
Bond Distances (Å) in 9R-$BaRuO_3$

| | | | |
|---|---|---|---|
| Ba(1)–O(1) (3 ×) | 2.996(1) | Ru(1)–Ru(2) | 2.527(1) |
| Ba(1)–O(2) (6 ×) | 2.884(5) | Ru(1)–O(1) (3 ×) | 1.9771(7) |
| Ba(1)–O(2) (3 ×) | 2.957(5) | Ru(1)–O(2) (3 ×) | 2.001(6) |
| Ba(2)–O(1) (6 ×) | 2.877(5) | Ru(2)–O(2) (6 ×) | 1.999(6) |
| Ba(2)–O(2) (6 ×) | 2.933(5) | O(1)–O(1) (4 ×) | 2.878(6) |
| | | O(1)–O(2) (4 ×) | 2.837(5) |
| | | O(2)–O(2) (2 ×) | 2.686(7) |
| | | O(2)–O(2) (2 ×) | 2.962(7) |

quality single crystals of 9R-$BaRuO_3$ have been obtained and we have thus refined the structural parameters from single-crystal intensities collected using a Bruker SMART CCD X-ray diffractometer. The results are reported in Tables 8 and 9. In 9R-$BaRuO_3$ the three octahedral strings are corner shared (Fig. 7a). In $Ba_4Ru_3O_{10}$ described both in monoclinic [29] and orthorhombic [54] cells, FSO $Ru_3O_{12}$ units are two-dimensionally connected via terminal corners to form corrugated layers (Fig. 7b). In $Ba_4ZrRu_3O_{12}$, the trimers are connected through a single layer of $ZrO_6$ octahedra

by corner sharing [55] (Fig. 7c). In these two Ru(IV) trioctahedra strings-containing compounds the Ru–Ru distances are comparable (Table 10). In $Ba_6Ru_3Cl_2O_{12}$, the MOD of Ru is +4.67, the Ru–Ru bonds within the $Ru_3O_{12}$ entities are significantly longer and comparable to the values obtained in $Ba_5Ru_3O_{12}$ which contains isolated $Ru_3O_{12}$ trioctahedra groups in which part of ruthenium was replaced by platinum [29] (Fig. 7d). In $Ba_5Ru_3O_{12}$, average Ru–O distances and valence bond calculations indicated that the trimeric unit corresponds to Ru(V)–Ru(IV)–Ru(V). In $Ba_6Ru_2PtO_{12}Cl_2$ [17] and $Ba_6Nb_2IrO_{12}Cl_2$ [19] metal ordering within the trimers unambiguously indicated a $M$(V)–$M$(IV)–$M$(V) repartition. In contrast, due to the fact that in $Ba_6Ru_3Cl_2O_{12}$ the average Ru(1)–O distance is slightly higher than the Ru(2)–O(2) distance, the valence bond sums calculations using $R_0 = 1.834$ for Ru(IV) [28] and $R_0 = 1.888$ for Ru(V) [29] does not permit to determine the charge repartition on the three sites. In fact another possibility is a substantial delocalization leading to charge averaging. Although the distortion of the central $Ru(2)O(2)_6$ octahedron is small, the terminal $Ru(1)O(2)_3O(1)_3$ octahedra are strongly distorted with, as generally observed in FSO di- or tri-octahedra units, three shortest distances with common oxygens and three longer with non-shared oxygens. Note that the difference between the two types of Ru–O bonds is particularly significant in the present oxychloride.

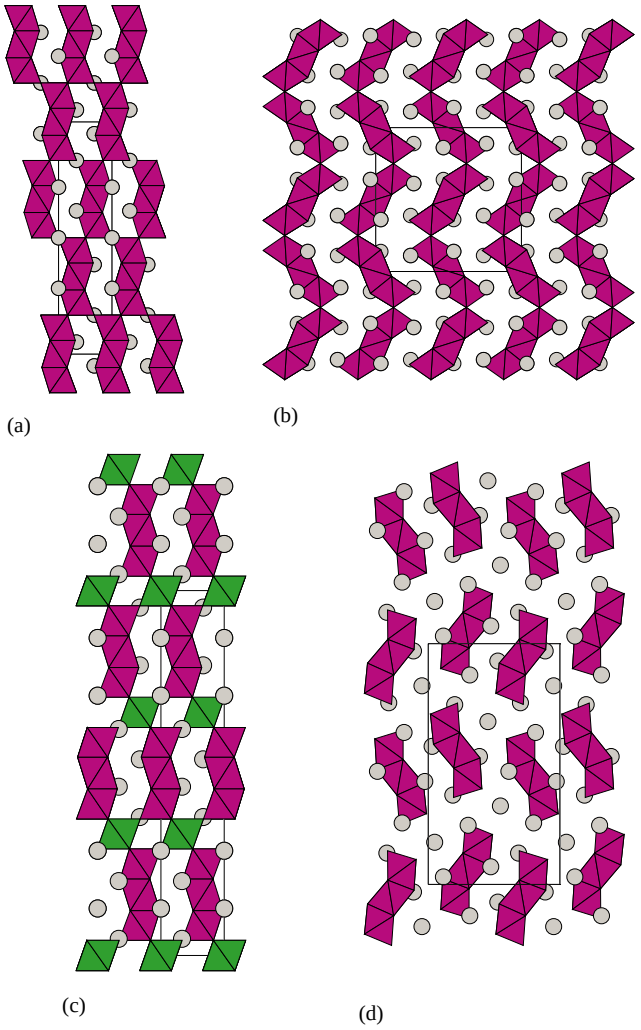


Fig. 7. Crystal structure of hexagonal perovskite-related compounds containing $Ru_3O_{12}$ strings of face shared octahedral: (a) 9R-$BaRuO_3$, (b) $Ba_4Ru_3O_{10}$, (c) $Ba_4ZrRu_3O_{12}$, and (d) $Ba_5Ru_3O_{12}$.

Many compounds have been obtained from the reaction of Ru or $RuO_2$ and $BaCO_3$ in $BaCl_2$ as a flux: 9R-$BaRuO_3$ ([46], this work), 4H-$BaRuO_3$ [46], O-$Ba_5Ru_2Cl_2O_9$ (O stands for orthorhombic) [22], H-$Ba_5Ru_2Cl_2O_9$ (H stands for hexagonal) (this work), $Ba_5Ru_2ClO_9$ [14], $Ba_6Ru_3Cl_2O_{12}$ (this work) and $Ba_7Ru_4Cl_2O_{15}$ [20]. The compounds H-$Ba_5Ru_2Cl_2O_9$, $Ba_6Ru_3Cl_2O_{12}$, and $Ba_7Ru_4Cl_2O_{15}$ are the terms $n = 2$, 3, 4 of the series $[Ba_2Cl_2]$ $[Ba_{n+1}M_nO_{3n+3}]$. The finding of "high pressure form" 4H-$BaRuO_3$ crystals, mixed with 9R-$BaRuO_3$ crystals in an ambient pressure preparation using $BaCl_2$ [46] could result from the rearrangement of some oxychlorides. In fact 9R-$BaRuO_3$ crystals could result from $Ba_6Ru_3Cl_2O_{12}$ by removing of the $Ba_2Cl_2$ layers and connecting the octahedra (with removing of the common $BaO_3$ layer) from two successive $[Ba_{n+1}M_nO_{3n+3}]$ slices (Fig. 8a). In this way, 4H-$BaRuO_3$ crystals could be obtained from H-$Ba_5Ru_2Cl_2O_9$, $Ba_5Ru_2ClO_9$ and $Ba_7Ru_4Cl_2O_{15}$

Table 10
Compounds containing $Ru_3O_{12}$ trimers made from face-shared $RuO_6$ octahedra

| Compound | Ru–Ru | $Ru_M$–$O_M$* | $Ru_T$–$O_M$* | $Ru_T$–$O_T$* | $\langle Ru_T–O \rangle$ | Ref. |
|---|---|---|---|---|---|---|
| $BaRuO_3$ | 2.55 | 2.00 | 2.02 | 1.96 | 1.99 | [51] |
| | 2.530 | 2.005 | 1.974 | 2.007 | 2.000 | [52] |
| | 2.543 | 1.984 | 2.056 | 1.967 | 2.011 | [53] |
| | 2.528 | 2.006 | 2.008 | 1.997 | 2.003 | This work |
| $Ba_4Ru_3O_{10}$ | 2.568/2.563 | 2.042/2.024 | 2.111/2.049 | 1.910/1.942 | 2.010/1.996 | [29,54] |
| $Ba_4ZrRu_3O_{12}$ | 2.529 | 2.009 | 2.013 | 1.974 | 1.993 | [55] |
| $Ba_5Ru_3O_{12}$ | 2.587/2.676 | 2.004 | 2.080/2.092 | 1.881/1.870 | 1.981/1.981 | [29] |
| $Ba_6Ru_3Cl_2O_{12}$ | 2.656 | 1.987 | 2.128 | 1.871 | 2.000 | This work |

*Label diagram for the $Ru_3O_{12}$ dimer $(O_T)_3$–$Ru_T$–$(O_M)_3$–$Ru_M$–$(O_M)_3$–$Ru_T$–$(O_T)_3$.

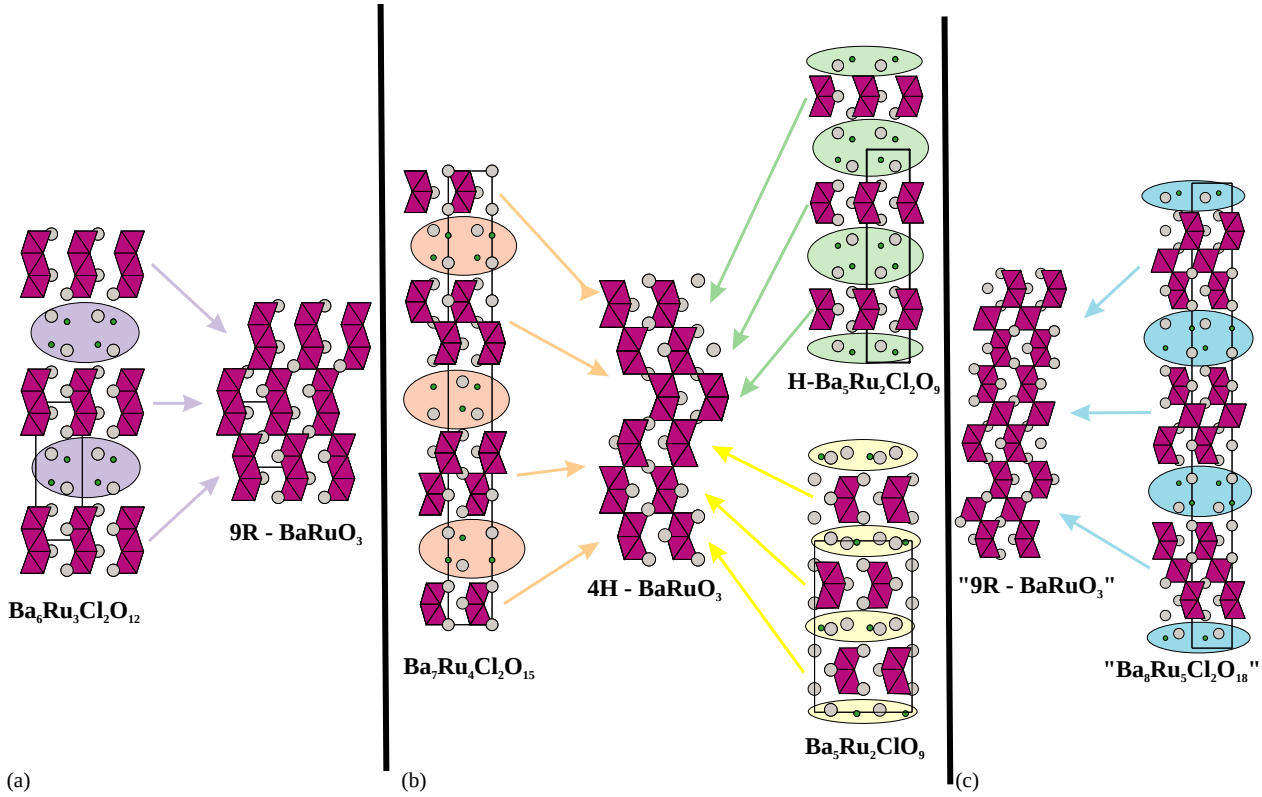


Fig. 8. Formation of various types of $BaRuO_3$ from $[Ba_2Cl_2]$ $[Ba_{n+1}Ru_nO_{3n+3}]$ by removing of the $Ba_2Cl_2$ layers. (a) 9R structure starting from $Ba_6Ru_3Cl_2O_{12}$, (b) 4H structure starting from $Ba_5Ru_2Cl_2O_9$, $Ba_5Ru_2ClO_9$ or $Ba_7Ru_4Cl_2O_{15}$, and (c) 15R structure starting from $Ba_8Ru_4Cl_2O_{18}$.

(Fig. 8b). Up today no single crystal of the term $n = 5$ of the $[Ba_2Cl_2]$ $[Ba_{n+1}Ru_nO_{3n+3}]$ series has been isolated, however, the corresponding compound $Ba_8Ru_{3.33}Ta_{1.67}Cl_2O_{18}$ with Ru and Ta disordered in the octahedra has been characterized [21]. Removal of the $Ba_2Cl_2$ layer from the ruthenium compound would result in a new form of $BaRuO_3$ with a 15R structure with $(hchcc)_3$ sequence of $BaO_3$ layers (Fig. 8c), this sequence has already been evidenced in $SrMn_{0.9}Fe_{0.1}O_3$ [56].

## 4. Conclusion

Single crystals of the terms $n = 2$ and 3 of the series $[Ba_2Cl_2]$ $[Ba_{n+1}Ru_nO_{3n+3}]$ have been isolated. The $[Ba_{n+1}Ru_nO_{3n+3}]$ slabs contain, respectively, $Ru_2O_9$ and $Ru_3O_{12}$ entities resulting from face-shared octahedra for $Ba_5Ru_2Cl_2O_9$ and $Ba_6Ru_3Cl_2O_{12}$, respectively. The mean oxidation state of Ru is +5 and +4.67, respectively. The term $n = 4$ has previously been reported and other terms are expected. Attempts to obtain intergrowth structures with mixed terms are also planed.

## References

[1] B. Aurivillius, Ark. Kemi. 1 (1949) 463.
[2] M. Dion, M. Ganne, M. Tournoux, Mater. Res. Bull. 16 (1981) 1429;
A.J. Jacobson, J.T. Lewandowski, J.W. Jhonson, J. Less-Common Met. 116 (1986) 137.
[3] S.N. Ruddlesden, P. Popper, Acta Crystallogr. 10 (1957) 538;
S.N. Ruddlesden, P. Popper, Acta Crystallogr. 11 (1958) 54.
[4] J.M. Longo, J.A. Kafalas, Mater. Res. Bull. 3 (1968) 687.
[5] J. Darriet, M.A. Subramanian, J. Mater. Chem. 5 (4) (1995) 543.
[6] L.M. Kovba, M.V. Paromova, Vestn. Mosk. Univ. Ser. Khim. 2 (1970) 621;
J. Krüger, Hk. Müller-Buschbaum, Rev. Chim. Miner. 20 (1983) 456;
J. Krüger, Hk. Müller-Buschbaum, Z. Anorg. Allg. Chem. 512 (1984) 59;
Hk. Müller-Buschbaum, M. Scheikowski, Z. Anorg. Allg. Chem. 591 (1990) 181;
Hk. Müller-Buschbaum, O. Schrandt, J. Alloys Compds. 191 (1993) 151.
[7] R.V. Shpanchenko, E.V. Antipov, L.N. Lykova, L.M. Kovba, Vestn. Mosk. Univ. Ser. Khim. 45 (1990) 29.
[8] R.V. Shpanchenko, A.M. Abakumov, E.V. Antipov, L.M. Kovba, J. Alloys Compds. 206 (1994) 185.
[9] K. Yamaura, P.D. Young, T. Siegrist, C. Besnard, C. Svensson, Y. Liu, R.J. Cava, J. Solid State Chem. 158 (2001) 175.
[10] N. Tancret, P. Roussel, F. Abraham, J. Solid State Chem., 2003, submitted for publication.
[11] C. Dussarat, J. Pompeyrine, J. Darriet, Eur. J. Solid State Inorg. Chem. 31 (1994) 289.
[12] F. Grasset, M. Zakhour, J. Darriet, J. Alloys Compds. 287 (1999) 25.
[13] F. Grasset, C. Dussarat, J. Darriet, J. Mater. Chem. 7 (9) (1997) 1911.

[14] M. Rath, Hk. Müller-Buschbaum, J. Alloys Compds. 209 (1994) 239.
[15] J. Wilkens, Hk. Müller-Buschbaum, J. Alloys Compds. 171 (1991) 255.
[16] S-T. Hong, A.W. Sleight, J. Solid State Chem. 132 (1997) 407.
[17] M. Neubacher, Hk. Müller-Buschbaum, Z. Anorg. Allg. Chem. 609 (1992) 59.
[18] M. Neubacher, Hk. Müller-Buschbaum, Z. Anorg. Allg. Chem. 602 (1991) 143.
[19] J. Wilkens, Hk. Müller-Buschbaum, J. Alloys Compds. 179 (1992) 187.
[20] J. Wilkens, Hk. Müller-Buschbaum, Acta Chem. Scand. 45 (1991) 812.
[21] J. Wilkens, Hk. Müller-Buschbaum, J. Alloys Compds. 184 (1992) 195.
[22] Ch. Lang, Hk. Müller-Buschbaum, Z. Anorg. Allg. Chem. 587 (1990) 39.
[23] SAINT Plus Version 6.22, Bruker Analytical X-ray Systems, Madison, WI, 2001.
[24] R. H. Blessing, SADABS2.03: Program for absorption correction using SMART CCD based on the method of Blessing, Acta Crystallogr. A 51 (1995) 33.
[25] A. Altomare, G. Cascaro, G. Giacovazzo, A. Guagliardi, M.C. Burla, G. Polidori, M. Gamalli, J. Appl. Crystallogr. 27 (1994) 135.
[26] V. Petricek, M. Dusek, JANA2000, Institute of Physics, Praha, Czech Republic, 2002.
[27] I.D. Brown, in: M. O'Keefe, A. Navrotsky (Eds.), Structure and Bonding in Crystals, Vol. II, Academic Press, New York, 1980, pp. 1–30.
[28] M.E. Brese, M. O'Keeffe, Acta Crystallogr. B 47 (1991) 192.
[29] C. Dussarat, F. Grasset, R. Bontchev, J. Darriet, J. Alloys Compds. 233 (1996) 15.
[30] I.D. Brown, D. Altermatt, Acta Crystallogr. B 41 (1985) 244.
[31] F. Abraham, J. Trehoux, D. Thomas, Mater. Res. Bull. 12 (1977) 43.
[32] F. Abraham, J. Trehoux, D. Thomas, Mater. Res. Bull. 13 (1978) 805;
A. Cotton, C.E. Rice, J. Solid State Chem. 25 (1978) 137.
[33] Y. Doi, M. Wakeshima, Y. Hinatsu, A. Tobo, K. Ohoyama, Y. Yamagushi, J. Mater. Chem. 11 (2001) 3135.
[34] D. Verdoes, H.W. Zandbergen, D.J.W. Ijdo, Acta Crystallogr. C 41 (1985) 170.
[35] Y. Doi, K. Matsuhira, Y. Hinatsu, J. Solid State Chem. 165 (2002) 317.
[36] Y. Doi, Y. Hinatsu, J. Mater. Chem. 12 (2002) 1792.
[37] M. Rath, Hk. Müller-Buschbaum, J. Alloys Compds. 210 (1994) 119.
[38] Y. Doi, Y. Hinatsu, Y. Shimojo, Y. Ishii, J. Solid State Chem. 161 (2001) 113.
[39] J.T. Rijssenbeek, Q. Huang, R.W. Erwin, H.W. Zandbergen, R.J. Cava, J. Solid State Chem. 146 (1999) 65.
[40] P. Lightfoot, P.D. Battle, J. Solid State Chem. 89 (1990) 174.
[41] J. Darriet, M. Drillon, G. Villeneuve, P. Hagenmuller, J. Solid State Chem. 19 (1976) 213.
[42] J. Darriet, J.L. Soubeyroux, A.P. Murani, J. Phys. Chem. Solids 44 (3) (1983) 269.
[43] H.W. Zandbergen, D.J.W. Ijdo, Acta Crystallogr. C 40 (1984) 919.
[44] K.E. Stitzer, M.D. Smith, W.R. Gemmill, H.-C. zur Loye, J. Am. Chem. Soc. 124 (2002) 13877.
[45] E. Quarez, M. Huvé, F. Abraham, O. Mentré, Solid State Sci. 5 (2003) 951.
[46] S-T. Hong, A.W. Sleight, J. Solid State Chem. 128 (1997) 251.
[47] P.D. Battle, S.H. Kim, A.V. Powell, J. Solid State Chem. 101 (1992) 161.
[48] J. Darriet, R. Bontchev, C. Dussarat, F. Weill, B. Darriet, Eur. J. Solid State Inorg. Chem. 30 (1993) 287.
[49] E. Quarez, O. Mentré, Solid State Sci. 5 (2003) 1105.
[50] E. Quarez, F. Abraham, O. Mentré, J. Solid State Chem., 2003, in press, Corrected proof, Available online 30 September 2003.
[51] P.C. Donohue, L. Katz, R. Ward, Inorg. Chem. 4 (3) (1965) 306.
[52] A. Santoro, I. Natali Sora, Q. Huang, J. Solid State Chem. 151 (2000) 245.
[53] M.V. Rama Rao, V.G. Sathe, D. Sornadurai, B. Panigrahi, T. Shripathi, J. Phys. Chem. Solids 62 (2001) 797.
[54] A.H. Carim, P. Dera, L.W. Finger, B. Mysen, C.T. Prewitt, D.G. Schlom, J. Solid State Chem. 149 (2000) 137.
[55] C.H. De Vreugd, H.W. Zandbergen, D.J.W. Ijdo, Acta Crystallogr. C 40 (1989) 1987.
[56] E.J. Cussen, J. Sloan, J.F. Vente, P.D. Battle, T.C. Gibb, Inorg Chem. 37 (1998) 6071.